Determination of the stellar (n,γ) cross section of ^{40}Ca with accelerator mass spectrometry

I. Dillmann,* C. Domingo-Pardo,† M. Heil,† and F. Käppeler
Forschungszentrum Karlsruhe, Institut für Kernphysik, Postfach 3640, D-76021 Karlsruhe, Germany

A. Wallner, O. Forstner, R. Golser, W. Kutschera, A. Priller, and P. Steier
Vienna Environmental Research Accelerator, Fakultät für Physik, Universität Wien, A-1090 Wien, Austria

A. Mengoni
International Atomic Energy Agency, Wagramer Strasse 5, A-1400 Wien, Austria

R. Gallino‡
Dipartimento di Fisica Generale, Università di Torino, Via P. Giuria 1, I-10125 Torino, Italy

M. Paul
Racah Institute of Physics, Hebrew University, IL-Jerusalem 91904, Israel

C. Vockenhuber
TRIUMF, 4004 Wesbrook Mall, Vancouver, B. C., V6T 2A3, Canada
(Received 2 April 2008; published 30 June 2009)

The stellar (n,γ) cross section of ^{40}Ca at $kT = 25$ keV has been measured with a combination of the activation technique and accelerator mass spectrometry (AMS). This combination is required when direct off-line counting of the produced activity is compromised by the long half-life and/or missing γ-ray transitions. The neutron activations were performed at the Karlsruhe Van de Graaff accelerator using the quasistellar neutron spectrum of $kT = 25$ keV produced by the ^{7}Li$(p,n)^{7}$Be reaction. The subsequent AMS measurements were carried out at the Vienna Environmental Research Accelerator (VERA) with a 3 MV tandem accelerator. The doubly magic ^{40}Ca is a bottle-neck isotope in incomplete silicon burning, and its neutron capture cross section determines the amount of leakage, thus impacting on the eventual production of iron group elements. Because of its high abundance, ^{40}Ca can also play a secondary role as "neutron poison" for the s-process. Previous determinations of this value at stellar energies were based on time-of-flight measurements. Our method uses an independent approach, and yields for the Maxwellian-averaged cross section at $kT = 30$ keV a value of $\langle\sigma\rangle_3 0$ keV $= 5.73 \pm 0.34$ mb.

DOI: 10.1103/PhysRevC.79.065805 PACS number(s): 25.40.Lw, 26.30.−k, 27.40.+z, 97.10.Cv

I. INTRODUCTION

The doubly magic ^{40}Ca is mainly produced in explosive burning processes during supernova explosions. In contrast to the "normal" hydrostatic burning phases, the respective explosive burning is only ignited for a few seconds when the supernova shock front passes through the outer layers. The main fuels for the explosive burning stages are the so-called α nuclei consisting of ^{4}He clusters (^{12}C, ^{16}O, ^{20}Ne, and ^{28}Si). The ignition temperatures are between 1.9 GK (for carbon burning) up to 4 GK (for silicon burning). The time scales of neon and silicon burning depend only on the respective temperatures and not on the density, since both are dominated by the photodisintegration reactions of ^{20}Ne(γ,α) and ^{28}Si(γ,α). Apart from its role in astrophysics, the (n,γ) cross section of ^{40}Ca represents an important test for the applicability of the Hauser-Feshbach statistical model in the limit of low level densities.

A. Production of ^{40}Ca

Woosley [1] showed already in 1973 that a superposition of explosive oxygen burning, complete silicon burning with α-rich freeze-out, and incomplete silicon burning offers good fits to the solar abundances in the mass region $28 < A < 62$.

In explosive oxygen burning, a quasistatistical equilibrium (QSE) in the mass range $A = 28$–45 is obtained at $T > 3$ GK [2–4]. This temperature is too low to achieve full nuclear statistical equilibrium (NSE), but in zones where the temperature exceeds 4 GK minor production of iron group elements can occur. The main burning products are the α nuclei ^{28}Si, ^{32}S, ^{36}Ar, and ^{40}Ca.

Explosive silicon burning occurs at $T > 4$–5 GK and can be subdivided into incomplete burning, complete burning with normal freeze-out, and complete burning with α-rich freeze-out. Complete Si burning is attained for $T > 5$ GK, where full NSE is established and the iron group elements are

*iris.dillmann@ph.tum.de; Present address: Physik Department E12 and Excellence Cluster Universe, Technische Universitt Mnchen, D-85748 Garching, Germany.
†Present address: Gesellschaft für Schwerionenforschung, Darmstadt, Germany.
‡Also at Centre for Stellar and Planetary Astrophysics, Monash University, Victoria 3800, Australia.

produced. Complete Si burning with α-rich freeze-out occurs at low densities when the triple α reaction is not fast enough to keep the helium abundance in equilibrium. Then traces of α nuclei remain which were not transformed into iron group elements.

Incomplete silicon burning occurs at peak temperatures of $T = 4$–5 GK when the temperature is not high enough for nuclear reactions to overcome the bottleneck at the proton-magic shell closure $Z = 20$. The most abundant burning products are the same as for explosive oxygen burning, but partial leakage can produce iron group elements such as ^{54}Fe and ^{56}Ni. Which of the three silicon burning scenarios actually takes place depends on the respective peak temperatures and densities during the passage of the supernova shock front.

B. Neutron poisons in massive stars

The neutrons for the *s*-process produced *in situ* by the ^{13}C$(\alpha,n)^{16}$O and ^{22}Ne$(\alpha,n)^{25}$Mg sources can be consumed by isotopes with high abundances A_i and/or large neutron capture cross sections. The most important "neutron poisons" are ^{16}O and ^{25}Mg, the products of the neutron source reactions. These isotopes reduce the available neutrons per ^{56}Fe seed and thus the *s*-process efficiency. Further neutron poisons are ^{17}O, ^{20}Ne, and ^{24}Mg. This list can also be extended to ^{40}Ca, since this doubly magic isotope exhibits both, a rather high solar abundance which reflects the high abundance in the preceding generation of stars (see Table I), and one of the largest Maxwellian averaged cross sections among the 20 most abundant isotopes.

For the reasons outlined above, an accurate knowledge of the neutron capture cross section of ^{40}Ca is of importance for the leakage through the $N = Z = 20$ bottleneck and for the role as possible neutron poison. The previous recommended Maxwellian-averaged cross section (MACS) of $\langle\sigma\rangle_{30\,\mathrm{keV}} = 6.7 \pm 0.7$ mb at $kT = 30$ keV [7] was taken directly from Musgrove *et al.* [8] and is essentially based on the respective resonance parameters measured below $E_n = 300$ keV, with contributions from the total neutron cross section measurement of Singh *et al.* [9], both using the time-of-flight (TOF) method.

The remeasurement of the ^{40}Ca$(n,\gamma)^{41}$Ca cross section with an independent method such as the activation technique plus following AMS could add confidence in these results. The very high sensitivity of the activation technique allows one to use very small samples so that neutron scattering corrections are completely negligible. A further advantage of the activation technique compared to the TOF method is that the direct capture component (DRC) is already included. In combination with accelerator mass spectrometry (AMS), this technique can be extended to hitherto inaccessible cases, where the product nuclei exhibit a long half-life and no γ-ray transitions (e.g., ^{41}Ca, $t_{1/2} = 103\,000$ yr [10,11]). Direct atom counting via AMS also avoids uncertainties associated with the γ-decay branching of the activation products.

In Sec. II we describe the experimental techniques of the activation with a stellar neutron source and the subsequent counting of the produced ^{41}Ca with accelerator mass spectrometry. Section III shows the data analysis, and the results are presented in Sec. IV. The astrophysical conclusions of our results are given in Sec. V.

TABLE I. Isotopic [5] and solar abundances A_i (relative to $A_{\mathrm{Si}} = 10^6$) [6] of the stable Ca isotopes.

Isotope	Isotopic abundance [%]	Solar abundance A_i
^{40}Ca	96.941(156)	59200
^{42}Ca	0.647(23)	395
^{43}Ca	0.135(10)	82.5
^{44}Ca	2.086(110)	1275
^{46}Ca	0.004(3)	2.4
^{48}Ca	0.187(21)	114
Σ_{Ca}	100	61068.9

II. EXPERIMENTAL TECHNIQUE

A. Activation

The activation was carried out at the Karlsruhe 3.7 MV Van de Graaff accelerator. Neutrons were produced with the ^{7}Li$(p,n)^7$Be source by bombarding 30μm thick layers of metallic Li on a water-cooled Cu backing with protons of 1912 keV, 30 keV above the reaction threshold. The angle-integrated neutron spectrum imitates almost perfectly a Maxwell-Boltzmann distribution for $kT = 25.0 \pm 0.5$ keV with a maximum neutron energy of 106 keV [12]. At this proton energy, the neutrons are kinematically collimated in a forward cone with 120° opening angle. Neutron scattering through the Cu backing is negligible, since the transmission is about 98% in the energy range of interest. To ensure homogeneous illumination of the entire surface, the proton beam with a direct current of ≈100 μA was wobbled across the Li target. Thus, the mean neutron intensity over the period of the activations was ≈1.0–1.6 × 10^9 s^{-1} at the position of the samples, which were placed in close geometry to the Li target. A ^{6}Li-glass monitor at a 1 m distance from the neutron target was used to record the time dependence of the neutron yield in intervals of 1 min as the Li target degraded during the irradiation. In this way the proper correction of the number of nuclei that decayed during the activation could be attained. This correction is negligible for very long half-lives, e.g., for ^{41}Ca, but becomes important for comparably short-lived isotopes and affects the determination of the ^{198}Au activity, since gold is used as the reference cross section for the neutron fluence determination.

A sample of calcium carbonate (152.6 mg $CaCO_3$, corresponding to 8.926 × 10^{20} atoms ^{40}Ca) with natural isotopic abundance (96.941% ^{40}Ca [13], see Table I) was used in this measurement. The sample material was pressed into a thin pellet 8 mm in diameter, enclosed in 15 μm thick aluminium foil, and sandwiched between two 30 μm thick gold foils of the same diameter. In this way, the neutron fluence in our experimental neutron distribution could be determined relative to the well-known capture cross section of ^{197}Au [12]. During the activation, the gold foils and Li targets were changed three times, subdividing the experiment into four single activations

TABLE II. Overview of the activation parameters. t_a is the irradiation time, and Φ_{tot} the total neutron exposure. For discussion of the uncertainties, see Sec. III C.

Activation	t_a (min)	Φ_{tot} ($\times 10^{14} n$)
Ca-a	4075	2.542
Ca-b	10078	7.085
Ca-c	9909	9.606
Ca-d	4123	4.008
Total	28185	23.242

(see Table II). The net irradiation time was ≈20 d, and the total neutron exposure was calculated using the activated gold foils to be 2.32×10^{15} neutrons.

B. AMS measurement

The number of ^{41}Ca nuclei produced in the neutron activation was measured offline applying the technique of accelerator mass spectrometry (AMS) at the VERA (Vienna Environmental Research Accelerator) facility. This facility is based on a 3-MV tandem accelerator equipped with a 40-sample caesium sputter source. Details on Ca measurements at VERA can be found in Refs. [14,15]. The sample material was sputtered in the ion source, and the nuclides were analyzed according to their mass and energy. Calcium fluoride (CaF_2) was chosen as the proper sputter material. It was shown to provide sufficiently large negative currents when extracting CaF_3^- ions, with the additional advantage that the production of the interfering isobar (KF_3^-) is strongly reduced [16–18].

After the neutron activation, the entire Ca-containing pellet ($CaCO_3$) was dissolved in nitric acid to ensure a uniform mixture of the irradiated sample material; consequently, a cross-section value integrated over the full sample area is obtained. Several aliquots were used to prepare sputter targets in the following way. Under pH control, hydrofluoric acid (HF) was added to the solution and Ca precipitated as CaF_2, separated via centrifugation, and then dried to get CaF_2 powder. After mixing with Cu powder, this material was pressed into the sample holders and inserted into the ion source. Overall, 17 sputter cathodes and a similar amount of identical but nonirradiated blank samples were prepared for the AMS measurements.

The ^{41}Ca content was determined during eight measurement series applying two different particle detection setups, thus reducing systematic uncertainties. AMS measures isotope ratios by determining the count rate of the rare isotope (^{41}Ca) relative to the ion current of a reference isotope (^{40}Ca). The procedure applied at VERA is the following. Negatively charged ions are mass separated and injected into a tandem accelerator, which runs at typically 3 MV. At the terminal, the particles have to pass a gas stripper canal where electrons are stripped off from the negative ions and parasitic molecular ions dissociated via collisions and Coulomb breakups in the gas. The resulting positive ions are further accelerated. After the tandem accelerator, the 4^+ charge state is selected; i.e., particles having energies of 13.5 MeV and the right mass to charge ratio (M/q) are further transported to the particle detection setup. The number of radionuclides is measured with an energy-sensitive detector, while the current of the stable ions is determined with Faraday cups. In the case of Ca, fast switching between stable isotopes and the radionuclide was applied at the injector magnet, and both ^{40}Ca and ^{42}Ca currents were registered. The isotope ratios of the unknown samples were compared with ratios of ^{41}Ca/^{40}Ca reference materials [19]. Blank samples, having negligible ^{41}Ca concentrations, were used as controls for the quantification of the background level.

Two different detection setups were used for these measurements, both with the goal of efficiently separating any possible interferences in the signal of the radioisotope ^{41}Ca with the isobar ^{41}K. The first uses the so-called delta TOF setup [20,21]. Here, the time-of-flight is measured for particles that pass a thick, but very homogeneous, passive absorber foil made of silicon nitride (Silson Ltd., UK). K and Ca can be discriminated thanks to their different energy loss in the absorber, which is reflected in a different velocity when leaving the foil. The second method utilizes a recent development at ETH Zurich/Paul Scherrer Institut (PSI) of a compact type of ionization chamber which provides a high resolution in the energy measurement [22]. Particles enter this detector through a sufficiently thick silicon nitride entrance foil, and isobars, dispersed in energy by the loss in the foil, are discriminated with a segmented anode via a ΔE-E measurement.

For the measurement of the (n,γ) cross section, we expected an isotope ratio ^{41}Ca/Ca of $\approx 10^{-11}$, which is well above the machine background of ^{41}Ca/Ca at VERA and the level of blank and calcium material used as targets for neutron activation. Both setups have been proven to provide a sufficient isobar suppression for our samples.

III. DATA ANALYSIS AND RESULTS

A. Determination of neutron flux

The measurement of the induced ^{198}Au activity after the irradiation was performed with a high purity germanium (HPGe) detector with a well-defined measuring position at a distance of 76 mm surrounded by 10 cm lead shielding. The absolute efficiency for the 411.8 keV γ line of the decay into ^{198}Hg was determined with a set of reference sources and yielded $\varepsilon_\gamma = 0.212\%$.

The total amount of activated ^{198}Au nuclei, N_{198}, at the end of the irradiation can be deduced from the number of events $C(t_m)$ in the particular γ-ray line at 411.8 keV registered in the HPGe detector during the measuring time t_m [23]. The factor t_w corresponds to the waiting time between the end of the irradiation and the start of the activity measurement:

$$N_{198} = \frac{C(t_m)}{\varepsilon_\gamma I_\gamma k_\gamma (1 - e^{-\lambda t_m}) e^{-\lambda t_w}}. \quad (1)$$

I_γ accounts for the relative γ intensity per decay of the 411.8 keV transition [$I_\gamma = 95.58(\pm 0.12)\%$ [24]]. For the measurement of the activated gold foils with the HPGe, the γ-ray self-absorption k_γ has to be considered [23]. This correction factor was 0.995 for all gold foils.

The number of activated sample atoms N_{act} is determined by

$$N_{act} = N_i \langle \sigma_{exp} \rangle (i) \Phi_{tot} f_b(i). \quad (2)$$

In this equation, $\langle \sigma_{exp} \rangle (i)$ is the cross section in the experimental neutron spectrum, and Φ_{tot} the total neutron flux. The factor

$$f_b = \frac{\int_0^{t_a} \phi(t) e^{-\lambda(t_a - t)}\, dt}{\int_0^{t_a} \phi(t)\, dt} \quad (3)$$

accounts for the decay of activated nuclei during the irradiation time t_a as well as for variations in the neutron flux. This factor is calculated from the neutron flux history recorded throughout the irradiation with the ^{6}Li glass detector at 1 m distance from the target. The reference value for the experimental ^{197}Au cross section in the quasistellar spectrum of the ^{7}Li$(p,n)^7$Be source is $\langle \sigma_{exp} \rangle (^{197}\text{Au}) = 586 \pm 8$ mb [12].

The time-integrated neutron flux $\Phi_{tot} = \int \phi(t)\, dt$ seen by the sample (Table II) is determined by averaging the neutron fluxes of the two gold foils enclosing the respective sample:

$$\Phi_{tot} = \frac{N_{198}}{N_{197} \langle \sigma_{exp} \rangle (^{197}\text{Au}) f_b}. \quad (4)$$

B. Determination of the isotopic ratio via AMS

Accelerator mass spectrometry determines the ratio of a radioactive isotope relative to one stable isotope of the same element. This measurement is carried out relative to reference standards with well-known isotopic ratios. In our case, we determined the ratio of ^{41}Ca versus ^{40}Ca, $R = \frac{N_{41}}{N_{40}}$.

Figure 1 shows the first and second energy loss signal from the ionization chamber measured with a blank sample and an irradiated sample with ^{41}Ca. The events from the quasistable isobar ^{41}K and the radioisotope ^{41}Ca can be clearly distinguished. With these settings, also ions with the same M/q as ^{41}Ca can reach the detector, such as ^{82}Se. However, as can be seen in the top part of Fig. 1, these events are well separated from the $A = 41$ signals.

The AMS measurements were repeated eight times. In the first six measurements, the deltaTOF technique was applied, and in the remaining two the compact ionization chamber (see Sec. II B). The isotope ratio $R = \frac{N_{41}}{N_{40}}$ from these measurements is $(1.34 \pm 0.07) \times 10^{-11}$. The uncertainty is due to the 5.2% error (1σ) from the AMS measurement.

One can determine the experimental cross section $\langle \sigma_{exp} \rangle$ for the ^{40}Ca(n,γ) reaction for our experimental neutron spectrum with the known total neutron exposure $\Phi_{tot} = 2.324 \times 10^{15}$ from Table II and Eq. (2):

$$\langle \sigma_{exp} \rangle (^{40}\text{Ca}) = \frac{N_{41}}{N_{40}} \frac{1}{\Phi_{tot} f_b}. \quad (5)$$

Since $\frac{N_{41}}{N_{40}}$ is the isotopic ratio R, and the correction factor f_b for very long half-lives is equal to unity, this equation simplifies to

$$\langle \sigma_{exp} \rangle (^{40}\text{Ca}) = R \frac{1}{\Phi_{tot}}. \quad (6)$$

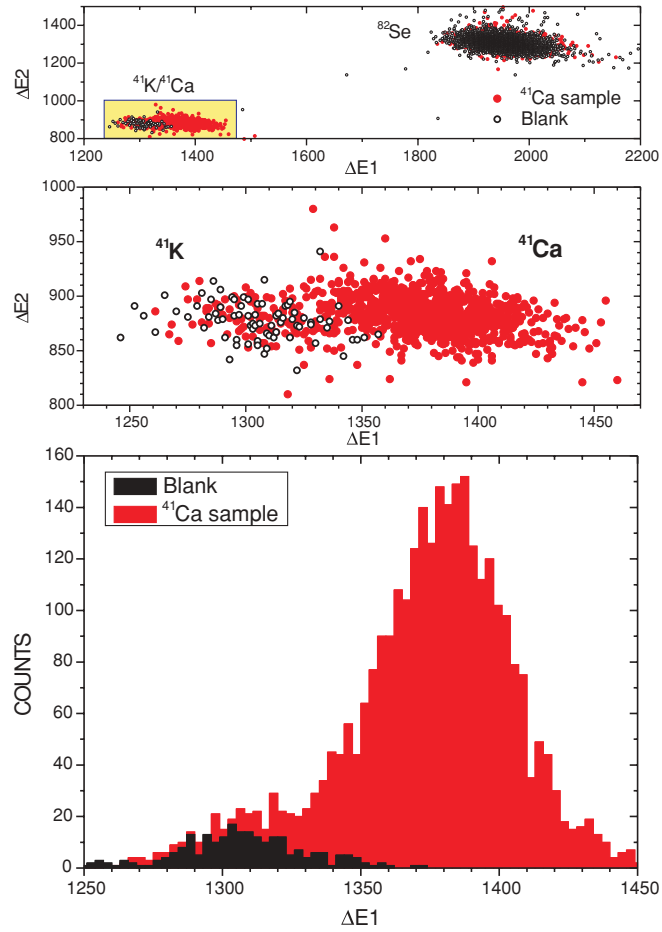

FIG. 1. (Color online) Top/middle: First ($\Delta E1$) and second ($\Delta E2$) energy loss signals from the anodes in the ionization chamber. The events from ^{41}Ca and its stable isobar ^{41}K can be distinguished by comparing a blank and an irradiated sample with ^{41}Ca. In the top panel events from ^{82}Se appear at higher energy losses which have the same M/q as ^{41}Ca. Bottom: Histogram illustrating the separation between ^{41}K and ^{41}Ca.

From this equation, we can deduce an experimental cross section of $\langle \sigma_{exp} \rangle (^{40}\text{Ca}) = 5.77 \pm 0.34$ mb (uncertainty including the total uncertainty from Table III).

C. Error analysis

The experimental uncertainties are summarized in Table III. Since stellar neutron capture cross section measurements are often carried out relative to gold [7], the error of 1.4% [12] in the gold cross section cancels out in most astrophysical applications and therefore was not included in the present error analysis. An error of 2.0% was assumed to account for the uncertainty of the sample position (0.25 mm) relative to the gold foils during the activation that affects the neutron flux seen by the sample. The uncertainty of the HPGe efficiency calibration was derived from the accuracy of the calibration sources and of the calibration procedure. The uncertainty (1σ) in the AMS measurements (5.2%) includes the statistical uncertainty, the reproducibility of the measurement, and a systematic contribution from the measurement relative to

TABLE III. Uncertainties for ^{197}Au and ^{40}Ca.

Source of uncertainty	Uncertainty (%)	
	^{197}Au	^{40}Ca
Gold cross section	1.4[a]	–
Detector efficiency	2.0	–
Neutron flux	2.0	–
Sample mass	0.4	–
γ-ray intensity	0.1	–
Counting statistics	0.2	–
AMS uncertainty	–	5.2
Total uncertainty	2.9	5.9[b]

[a]Not included in the final uncertainty, see text.
[b]Including the 2.9% uncertainty from the flux measurement with the gold samples.

reference materials (which is dominated by the uncertainty of the half-life of ^{41}Ca). The total uncertainty of 5.9% is the combination of the uncertainties from the neutron flux measurement (2.9%) and the AMS measurement (5.2%).

IV. CROSS SECTIONS

A. Evaluated cross section libraries

The energy-dependent neutron cross sections from the evaluated cross section libraries JEFF-3.0A, JEFF-3.1, ENDF/B-VII.0, and JENDL-3.3 include experimental resonance parameters adopted from the compilations of Mughabghab [25,26]. These parameters were determined in a TOF measurement by Musgrove [8] in the energy range between 2.5 and 300 keV with contributions from the total neutron cross section measurement of Singh *et al.* [9]. The quoted uncertainty for most resonance parameters from Musgrove [8] is of the order of 10% and larger.

The unresolved resonance region above 296 keV is based on different statistical model calculations and thus differs from evaluation to evaluation. For example, in JENDL-3.3 this region originates from the code CASTHY [27] and was normalized to the Maxwellian average $\langle\sigma\rangle_{30\,\mathrm{keV}} = 6.7$ mb given in Ref. [7]. The data sets of JEFF-3.1 and ENDF/B-VII.0 are identical and use the recent nuclear model code TALYS [28], where the parameters have been adjusted to reproduce the existing experimental data. However, for the calculation of Maxwellian cross sections up to $kT = 100$ keV, the contribution from the unresolved resonance region has only little influence, and we used an average of all four data sets.

B. Maxwellian averaged cross sections

In an astrophysical environment with temperature T, interacting particles are quickly thermalized by collisions in the stellar plasma, and the neutron energy distribution can be described by a Maxwell-Boltzmann spectrum as

$$\Phi = dN/dE_n \sim \sqrt{E_n}e^{-E_n/kT}. \quad (7)$$

The experimental neutron spectrum of the ^{7}Li$(p,n)^7$Be reaction simulates the energy dependence of the flux $v\Phi \sim E_n e^{-E_n/kT}$ with $kT = 25.0 \pm 0.5$ keV almost perfectly [12]. However, the cutoff at $E_n = 106$ keV and small deviations from the shape of the ideal Maxwellian spectrum require a correction of the measured cross section $\langle\sigma_{\mathrm{exp}}\rangle$ for obtaining a true Maxwellian average, $\langle\sigma\rangle_{25\,\mathrm{keV}}$. This correction is determined by means of the energy-dependent cross sections from data libraries.

Before calculating a Maxwellian averaged cross section, we determine a "normalization factor" NF which gives a direct comparison of how good the agreement is between our measured cross sections $\langle\sigma_{\mathrm{exp}}\rangle$ and the evaluated cross sections $\sigma(E)$ folded with the experimental neutron spectrum of the ^{7}Li$(p,n)^7$Be source [12], $\langle\sigma_{\mathrm{eval}}\rangle = 5.18$ mb. Our experimentally determined cross section is $\langle\sigma_{\mathrm{exp}}\rangle = 5.77$ mb, resulting in a normalization factor of $NF = \frac{\langle\sigma_{\mathrm{exp}}\rangle}{\langle\sigma_{\mathrm{eval}}\rangle} = 1.11$.

The respective cross section derived by folding the NON-SMOKER energy dependence [29,30] with our experimental neutron distribution would be $\langle\sigma_{\mathrm{NS}}\rangle = 12.48$ mb, yielding a normalization factor of $NF = 0.46$. The Hauser-Feshbach model cannot be applied below a given minimum energy of $kT \approx 40$ keV ($T_9 \approx 0.48$ GK) [30] because of the low level density of the doubly magic nucleus ^{40}Ca which causes an overestimation of cross sections. Such low level densities occur also for very neutron- or proton-rich isotopes close to the drip lines, with low mass nuclei, and at low energies.

Applying the normalization factor NF to the evaluated libraries affects also the corresponding thermal value and the strength of the individual resonances. However, since the uncertainty of the resonance parameters is, as mentioned above, 10% and larger, we decided to use this approach. As soon as more accurate resonance parameters become available for ^{40}Ca, these data should supersede our way of extrapolating Maxwellian cross sections via Eq. (8):

$$\langle\sigma\rangle_{kT} = \frac{2}{\sqrt{\pi}} \frac{\int \frac{\sigma(E_n)}{NF} E_n e^{-E_n/kT}\, dE_n}{\int E_n e^{-E_n/kT}\, dE_n}. \quad (8)$$

The factor $2/\sqrt{\pi}$ comes from the normalization of the Maxwellian flux formula when using the most probable velocity instead of the mean thermal velocity. At $kT = 30$ keV this yields $\langle\sigma\rangle_{30\,\mathrm{keV}} = 5.73 \pm 0.34$ mb with our experimentally derived normalization factor $NF = 1.11$.

We have also recalculated the Maxwellian averaged cross sections using the resonance parameters given in ENDF/B-VII.0 [31] with the R-matrix analysis code SAMMY [32], yielding $\langle\sigma\rangle_{30\,\mathrm{keV}} = 5.13$ mb at $kT = 30$ keV. A calculation of the uncertainties was done independently by Monte Carlo sampling of the four most important resonance parameters which contribute 85.3% to the Maxwellian average at $kT = 30$ keV. Varying the resonances at $E_n = 10.83, 20.43, 42.12$, and 52.57 keV within their given uncertainties yielded $\langle\sigma\rangle_{30\,\mathrm{keV}} = 5.04 \pm 0.30$ mb. Varying the neutron widths Γ_n of all resonances by 5% and the respective γ widths Γ_γ by 20% gives $\langle\sigma\rangle_{30\ \mathrm{keV}} = 5.16 \pm 0.31$ mb, in perfect agreement with the SAMMY calculation.

In Table IV, these values are compared with the previously recommended values from Bao *et al.* [7], which were adopted from Ref. [33] and originate directly from Ref. [8]. As can be seen in Table IV and also in the graphical comparison of the

TABLE IV. Maxwellian averaged cross sections $\langle\sigma\rangle_{kT}$ (in mb) for ^{40}Ca calculated with the energy dependencies from evaluated libraries ("This work"). The second column shows the previous recommended values [7,33] based on the value from Ref. [8]; the third column lists the results calculated with resonance parameters in ENDF/B-VII.0 [31].

kT (keV)	$\langle\sigma\rangle_{kT}$ (mb)		
	This work	Refs. [7,8,33]	Ref. [31]
5	11.96	11.3	10.79
10	11.49	12.1	10.35
15	9.23	10.3	8.31
20	7.56	8.6	6.81
25	6.46	7.5	5.81
30	5.73(34)	6.7(7)	5.16(31)
40	4.93	5.8	4.44
50	4.53	5.4	4.08
60	4.28	5.2	3.85
80	3.91	4.9	3.51
100	3.59	4.9	3.19

energy trends in Fig. 3, the differences between the values from Refs. [7,8,33] and the recalculated Maxwellian cross sections increase with increasing temperature.

C. Comparison with previous values

Table V compares in the upper part the extrapolated Maxwellian averaged cross sections at $kT = 30$ keV from the evaluated library ENDF/B-VII.0 [31] (using data from Musgrove [8] and Singh [9]), Barrett [34], and the Bao *et al.* compilation [7,33] (taken directly from Ref. [8]) with our activation cross section. In the lower part of Table V the results from four Hauser-Feshbach predictions are given. Incidentally, the value of Woosley [35] agrees best with our experimental value of 5.73 ± 0.34 mb, but the recalculated value from the resonance parameters ($\langle\sigma\rangle_{30\,\mathrm{keV}} = 5.16 \pm 0.31$ mb) also agrees within the uncertainties. The large discrepancies to recent NON-SMOKER [29,30] and MOST [36,37] results indicate in the present case the limited reliability of the statistical model in view of the low level density in the doubly magic nucleus ^{40}Ca in this energy region.

D. Statistical model and direct capture calculations

Despite the fact that the Hauser-Feshbach model cannot (or only with large uncertainties) be applied below $kT \approx 40$ keV, we have performed statistical model calculations using the code HFSM with standard optical model parameters from Moldauer [38,39]. The level density is based on the Fermi gas theory with pairing and shell corrections. The parameters were fitted to reproduce the average level spacings of Mughabghab [25], e.g., for s waves $\langle \mathrm{D}(l=0)\rangle = 45 \pm 4$ keV. The giant dipole resonance parameters for the calculation of the average radiative widths were $E = 20.14$ MeV with a width of 8.05 MeV and a peak cross section of 58.3 mb. These values yield an average radiative width of $\langle\Gamma_\gamma\rangle_s = 193$ meV,

TABLE V. Comparison of Maxwellian averaged cross sections at $kT = 30$ keV from previous experiments and theoretical predictions. Theoretical values are given without error bars.

Reference	$\langle\sigma\rangle_3$0 keV (mb)	Ratio to this work
This work	5.73 (34)	–
ENDF/B-VII.0 [31]	5.16 (31)	$0.90^{+0.11}_{-0.10}$
Barrett [34]	10 (3)	$1.75^{+0.67}_{-0.59}$
Bao *et al.* [7,8,33]	6.7 (7)	$1.17^{+0.20}_{-0.18}$
Woosley [35]	5.8	$1.01^{+0.06}_{-0.06}$
NON-SMOKER [29]	13.0	$2.27^{+0.14}_{-0.13}$
MOST (2002) [36]	24.1	$4.21^{+0.27}_{-0.24}$
MOST (2005) [37]	13.9	$2.43^{+0.15}_{-0.14}$

which is a factor of ≈8 lower than the 1.5 ± 0.9 eV from Musgrove [8]. However, only with this value can reasonable Maxwellian averaged cross sections be obtained. This decrease is interesting since the large difference of almost one order of magnitude to the average p- and d-wave widths ($\langle\Gamma_\gamma\rangle_p = 360 \pm 90$ meV and $\langle\Gamma_\gamma\rangle_d = 740 \pm 360$ meV) discussed in Ref. [8] vanishes.

Additional calculations were performed with the data set of ENDF/B-VII.0 [31], based on the evaluation of Mughabghab [25,26], and with the model code TALYS [28] for cross-checking. The results are consistent within a few percent for energies up to 10 keV, but differ by up to 20% for higher energies. TALYS calculations were repeated using a coupled-channel code, but this did not influence the neutron capture cross section. Thus the different energy dependencies from ENDF/B-VII.0 and TALYS originated only from the different optical model potentials used (Fig. 2).

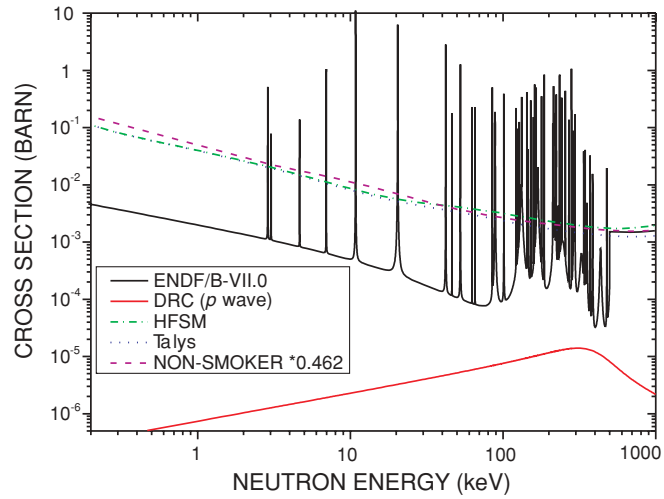

FIG. 2. (Color online) Energy-dependent cross sections $\sigma(E)$ for ^{40}Ca from the evaluated data library ENDF/B-VII.0 (black line) in comparison with the prediction from the Hauser-Feshbach models HFSM, NON-SMOKER (normalized by a factor of 0.462 to reproduce the experimental cross section), and TALYS. The red line in the lower part shows the DRC contribution from p-wave neutrons.

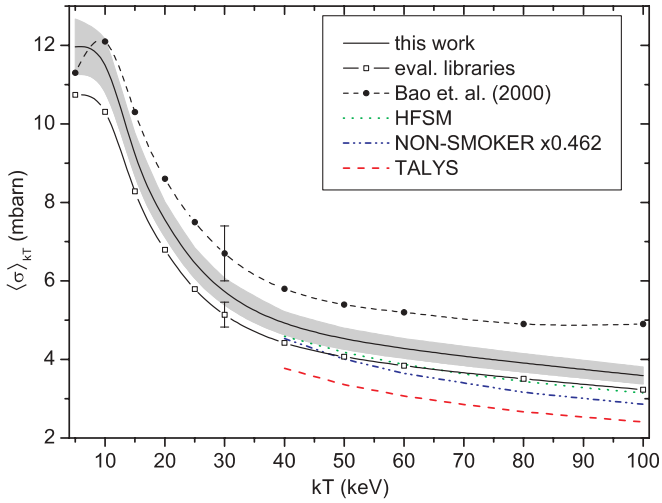

FIG. 3. (Color online) Maxwellian averaged cross sections from this work compared with previously recommended values [7,8,33] and the values calculated from resonance parameters of ENDF/B-VII.0 [31] (Table IV). The error band corresponds to the 5.9% uncertainty of our present measurement. Also plotted are the results obtained from the HF calculations HFSM and TALYS, and the normalized NON-SMOKER predictions.

Direct radiative capture (DRC) calculations have been performed for s- and p-wave neutron transitions to several bound states in ^{41}Ca. Using the experimental thermal cross section of $\sigma_{\rm th} = 410 \pm 20$ mb [26] and subtracting the contribution of 13.5 mb from the tail of the s-wave resonances, the estimated DRC cross section is 396.5 mb. The extrapolation from thermal energies to the keV region leads to very small DRC contributions of 0.4 mb and 5.4 μb for s- and p-wave neutrons at $kT = 25$ keV, respectively.

The best estimate for the Maxwellian averaged cross sections in the keV region can thus be obtained directly from the resonance parameters given in Refs. [25,26] normalized to the present results. For neutron energies below $E_n = 100$ keV, Maxwellian cross sections are determined by single resonances, and the Hauser-Feshbach theory cannot be applied. The predicted Maxwellian averaged cross sections in Fig. 3 should therefore be taken with care and are only plotted for $kT > 40$ keV.

V. CONCLUSIONS

We have measured the ^{40}Ca(n,γ) cross section via the activation technique in a stellar neutron distribution and derived a Maxwellian averaged cross section of $\langle\sigma\rangle_3 0$ keV $= 5.73 \pm 0.34$ mb at $kT = 30$ keV. This value is, within the error bars, in good agreement with the previously recommended value of 6.7 ± 0.7 mb [7,33] taken directly from Ref. [8], and higher than the value calculated from the resonance parameters [31], $\langle\sigma\rangle_{30\,\rm keV} = 5.16 \pm 0.31$ mb. With this result, ^{40}Ca still acts as a significant neutron poison in stellar environments, simply because of its high initial abundance. In the direct s-process flow, ^{40}Ca is bypassed by its quasistable isobar ^{40}K. In thermally pulsing low mass AGB stars [40], ^{40}Ca is therefore depleted by 13% in the s-process. However, the further reaction flow via ^{41}Ca can reach equilibrium. Accordingly, (n,γ) reactions on ^{40}Ca contribute to the overall s-process efficiency in the Ca to Cr region. This holds also for the s-process in massive stars, since the role as a neutron poison is not affected by (γ,n) reactions, even at the high temperatures during C shell burning.

ACKNOWLEDGMENTS

We thank E.-P. Knaetsch, D. Roller, and W. Seith for their help and support during the irradiations at the Van de Graaff accelerator. I.D. was supported by the Swiss National Science Foundation Grants 2024-067428.01 and 2000-105328. This work was supported by the Italian MIUR-PRIN 2006 Project "Final Phases of Stellar Evolution, Nucleosynthesis in Supernovae, AGB Stars, Planetary Nebulae."

[1] S. Woosley, W. Arnett, and D. Clayton, Astrophys. J. Suppl. Ser. **26**, 231 (1973).
[2] B. Meyer, T. Krishnan, and D. Clayton, Astrophys. J. **462**, 825 (1996).
[3] B. Meyer, T. Krishnan, and D. Clayton, Astrophys. J. **498**, 808 (1998).
[4] C. Freiburghaus, F. Rembges, T. Rauscher, E. Kolbe, F.-K. Thielemann, K.-L. Kratz, B. Pfeiffer, and J. Cowan, Astrophys. J. **516**, 381 (1999).
[5] J. de Laeter, J. Böhlke, P. de Bievre, H. Hidaka, H. Peiser, K. Rosman, and P. Taylor, Pure Appl. Chem. **75**, 683 (2003).
[6] E. Anders and N. Grevesse, Geochim. Cosmochim. Acta **53**, 197 (1989).
[7] Z. Bao, H. Beer, F. Käppeler, F. Voss, K. Wisshak, and T. Rauscher, At. Data Nucl. Data Tables **76**, 70 (2000).
[8] A. d. L. Musgrove, B. Allen, J. Boldeman, D. Chan, and R. Macklin, Nucl. Phys. **A259**, 365 (1976).
[9] U. Singh, H. Liou, J. Rainwater, G. Hacken, and J. Garg, Phys. Rev. C **10**, 2143 (1974).
[10] M. Paul, I. Ahmad, and W. Kutschera, Z. Phys. A **340**, 249 (1991).
[11] W. Kutschera, I. Ahmad, and M. Paul, Radiocarbon **34**, 436 (1992).
[12] W. Ratynski and F. Käppeler, Phys. Rev. C **37**, 595 (1988).
[13] K. Rosman and P. Taylor, Pure Appl. Chem. **70**, 217 (1998).
[14] A. Wallner, R. Golser, W. Kutschera, A. Priller, P. Steier, and C. Vockenhuber, Eur. Phys. J. A **27**, 337 (2006).
[15] A. Wallner, I. Dillmann, R. Golser, F. Käppeler, W. Kutschera, M. Paul, A. Priller, P. Steier, and C. Vockenhuber, Nucl. Instrum. Methods B **259**, 677 (2007).
[16] D. Fink, R. Middleton, J. Klein, and P. Sharma, Nucl. Instrum. Methods B **47**, 79 (1990).
[17] A. Urban, G. Korschinek, and E. Nolte, in *Workshop and Techniques in Accelerator Mass Spectrometry*, edited by R. Hedges and E. Hall (Oxford University, Oxford, UK, 1986) p. 108.
[18] P. Kubick and D. Elmore, Radiocarbon **31**, 324 (1989).

[19] K. Nishiizumi, M. Caffee, and D. DePaolo, Nucl. Instrum. Methods B **172**, 399 (2000).
[20] C. Vockenhuber, R. Golser, W. Kutschera, A. Priller, P. Steier, K. Vorderwinkler, and A. Wallner, Nucl. Instrum. Methods B **240**, 490 (2005).
[21] P. Steier, R. Golser, W. Kutschera, A. Priller, C. Vockenhuber, A. Wallner, and S. Winkler, Nucl. Instrum. Methods B **240**, 445 (2005).
[22] M. Suter, S. Jacob, and H.-A. Synal, Nucl. Instrum. Methods B **172**, 144 (2000).
[23] H. Beer and F. Käppeler, Phys. Rev. C **21**, 534 (1980).
[24] Z. Chunmei, Nucl. Data Sheets **95**, 59 (2002).
[25] S. Mughabghab, M. Divadeenam, and N. Holden, *Neutron Cross Sections*, BNL-325, 1st ed. (US Government Printing Office, Washington, 1981).
[26] S. Mughabghab, *Atlas of Neutron Resonances*, 5th ed. (Elsevier, New York, 2006).
[27] S. Igarasi and T. Fukahori, JAERI 1321, 1991 (unpublished).
[28] A. Koning, S. Hilaire, and M. Duijvestijn, TALYS version 0.56, 2004 (unpublished).
[29] T. Rauscher and F.-K. Thielemann, At. Data Nucl. Data Tables **75**, 1 (2000).
[30] T. Rauscher, HTML Interface to NON-SMOKER, 2009; online: http://nucastro.org/nonsmoker.html.
[31] M. Chadwick *et al.*, Nucl. Data Sheets **107**, 2931 (2006).
[32] N. Larson, Updated Users' Guide for SAMMY: Multilevel R-matrix Fits to Neutron Data Using Bayes' Equations, SAMMY Computer Code, ORNL/TM-9179/R7, Oak Ridge National Laboratory, 2006 (unpublished).
[33] H. Beer, F. Voss, and R. Winters, Astrophys. J. Suppl. Ser. **80**, 403 (1992).
[34] A. R. de L. Musgrove, B. J. Allen, J. W. Boldeman, D. M. H. Chan, and R. L. Macklin, Nucl. Phys. **A259**, 365 (1976).
[35] S. Woosley, W. Fowler, J. Holmes, and B. Zimmerman, At. Data Nucl. Data Tables **22**, 371 (1978).
[36] S. Goriely, Hauser-Feshbach rates for neutron capture reactions (version 09/12/02), http://www-astro.ulb.ac.be/Html/hfr.html (2002).
[37] S. Goriely, Hauser-Feshbach rates for neutron capture reactions (version 08/26/05), http://www-astro.ulb.ac.be/Html/hfr.html (2005).
[38] P. Moldauer, Nucl. Phys. **47**, 65 (1963).
[39] P. Moldauer, Rev. Mod. Phys. **36**, 1079 (1964).
[40] R. Gallino, C. Arlandini, M. Busso, M. Lugaro, C. Travaglio, O. Straniero, A. Chieffi, and M. Limongi, Astrophys. J. **497**, 388 (1998).